Journal of Hydrology 679 (2026) 136200

Contents lists available at ScienceDirect

Journal of Hydrology

journal homepage: www.elsevier.com/locate/jhydrol

Hierarchical water partitioning across different scales in sloped field: evidenced by soil pore water isotopic signatures

Jinzhuo Li [a,b,c], Xianwen Li [d], Mo Li [e], Liu Liu [f], Xiaorong Wei [b], Yaxian Hu [a,b,*]

[a] The Research Center of Soil and Water Conservation and Ecological Environment, Chinese Academy of Sciences and Ministry of Education, Yangling, Shaanxi 712100, China

[b] State Key Laboratory of Soil and Water Conservation and Desertification Control, Northwest A&F University, Yangling, Shaanxi 712100, China

[c] University of Chinese Academy of Sciences, Beijing 100049, China

[d] Key Laboratory of Agricultural Soil and Water Engineering in Arid and Semiarid Areas, Ministry of Education, Northwest A&F University, Yangling, Shaanxi 712100, China

[e] School of Water Conservancy and Civil Engineering, Northeast Agricultural University, Harbin, Heilongjiang, China

[f] State Key Laboratory of Efficient Utilization of Agricultural Water Resources, China Agricultural University, Beijing, China

ARTICLE INFO

Keywords:
Soil pore water
Stable isotopes
Hillslope hydrology
D-excess
Water partitioning

ABSTRACT

Soil pore water is like blood cycling in soil and plant system. However, beyond enrichment or depletion in bulk water content, we know little about how the heterogeneous turnover rates of soil water in differently sized pores affect or are affected by slope-scale water cycling. In this study, a Mollisol was collected from the Upper, Middle and Lower position along a typical rolling slope. At each position, bulk soil cores were sampled from three depths (10, 20, and 45 cm), and respectively centrifuged to step-wisely collect soil water stored in five differently sized pores. After comparing the stable isotopic signatures of H and O (δ^2H and $\delta^{18}O$) in each soil pore water, we observed that: (1) On average, > 83.5% of soil water was stored in pores < 6 μm, with stronger predominance at the Lower slope position and 45 cm deep. (2) Pore water δ^2H and $\delta^{18}O$ decreased with slope positions and depth, jointly resulting in enhanced Deuterium excess (d-excess) by 5.67‰ at the Lower slope position and by 3.56‰ at 45 cm deep. (3) Pore water δ^2H and $\delta^{18}O$ generally increased as pores became finer, and the d-excess maximized at 5.13‰ in Mesopores but minimized at –0.7‰ in Fine pores. The heterogeneous isotopic signatures and d-excess suggested that soil pore water did not cycle at the same rate but much more slowly in finer pores, resulting in much more advanced evaporative fractionation in smaller pores. Soil pores restructuring along the slope and profile, together with unequal evaporative fractionation and infiltration recharge, may have collectively contributed to the enhanced d-excess at Lower slope position and deeper layer. This is the first pore-scale evidence to decipher how water was partitioned across different spatial scales along hillslopes.

1. Introduction

Soil pore water is the principal storage and transport medium in the terrestrial water cycle (Vereecken et al., 2022), decisively regulating how precipitation is partitioned among evapotranspiration, infiltration and lateral runoff (Fatichi et al., 2020; Bonetti et al., 2021). Although soil water has been repeatedly monitored and modeled (Romano, 2014), most previous studies have represented it as a bulk scale variable, such as volumetric or gravimetric water content (Fatichi et al., 2020). Such bulk representation falls short when attempting to resolve the spatial heterogeneity of soil water stored in different pore domains, where water retention time and bioavailability may vary substantially (Rabot et al., 2018; Schlüter et al., 2020). As proposed in the "Two Water Worlds" hypothesis (Renée Brooks et al., 2010; McDonnell, 2014), the highly mobile water in Macropores (e.g., > 34 μm) and the tightly bound water in Micropores (e.g., < 6 μm) differ substantially in cycling rates and thus ecological functions (Radolinski et al., 2021). Hence, root water uptake, evaporative fractionation, and preferential flow do not act uniformly on the entire soil water reservoir. Instead, their effects are closely associated with the heterogeneous distribution and connectivity of water across different pore-size classes (Sprenger et al., 2017). Further zooming out in the field, repeated tillage practices, seasonal

* Corresponding author at: State Key Laboratory of Soil and Water Conservation and Desertification Control, Northwest A&F University, Yangling, Shaanxi 712100, China.

E-mail address: huyaxian@nwafu.edu.cn (Y. Hu).

https://doi.org/10.1016/j.jhydrol.2026.136200
Received 9 June 2026; Received in revised form 5 August 2026; Accepted 6 August 2026
Available online 8 August 2026

rainfall and erosion events may further heterogenize the soil pore structure and thus pore water retention time through soil profiles and over topographic positions (Chandrasekhar et al., 2018; Chen et al., 2021), mostly by the unequal evaporative fractionation and recharge rates introduced by prevailing processes such as runoff and infiltration (Knighton et al., 2019; Jarecke et al., 2021). Nevertheless, despite such broadly reconciled importance to distinguish soil water storage and availability across pore classes, it lacks a holistic framework as to quantitatively identify the hierarchical water partitioning across different pore domains, soil depths and topographic positions in sloped field.

In general, Macropores serve as the main pathways for preferential flow and facilitate rapid infiltration and drainage (Beven and Germann, 2013), whereas the water in Micropores constrained by capillary and adsorptive forces has limited mobility and slow turnover rates, and thus functions as an important storage pool (Wardak et al., 2022). However, the amount of soil water that can be effectively used by crops remains highly variable in both space and time (Zhao et al., 2018), given that the water potential range available for crop water uptake generally varies from –0.03 to –1.5 MPa (Nasta et al., 2023). Such variability is largely controlled by soil texture and structure (He et al., 2022), crop type, and seasonal changes (Liu et al., 2023a). For instance, coarse-textured or poorly structured soils tend to route more water through connected large pores, limiting retention in crop-accessible Mesopores (Rabot et al., 2018), vice versa for finer-textured or well-aggregated soils (De Lima et al., 2022; Henrique Novotny et al., 2023). Among crops, lucerne can exploit deeper pore water unavailable to wheat (Gaiser et al., 2012), whereas barley can maintain uptake from more saline and lower-potential pore domains than rice (Reddy et al., 2017; Munns et al., 2020). Sprenger et al. (2019) also claimed that the mobile and tightly bound water in a silty loam soil did not mix well despite intense rainfall events and high soil wetness (new water), but very likely being slowly rewetted with isotopically depleted winter/spring rain (old water). Apart from these inherent soil and crop properties, soil pore water cycling is also influenced by and meanwhile participates in local water redistribution across soil depth (Sprenger et al., 2017) and topographic positions (Jarecke et al., 2021). For instance, through soil profile, soil water stored in the upper layer exchanges more frequently with the atmosphere (i.e., via precipitation and evaporation), whereas the deeper soil received water through percolation and remains relatively isolated with limited evaporation and thus slower turnover rates (Floriancic et al., 2024). Across different topographic positions, apart from the erosional induced selective soil particle redistribution and pore restructure (Li et al., 2021), local soil water cycling is more regulated by runoff transport and lateral subsurface flow (Chen et al., 2021), thereby resulting in systematic differences in recharge frequency and residence time between upper and lower slope positions (Knighton et al., 2019). Yet, no matter how well understood in theory, we lack quantitative evidence to distinguish the relative role of soil pore water turnover rates, infiltration, evaporation and topographic redistribution at different scales in hillslope water cycling.

Although some widely applied conventional physical approaches, such as soil water retention curves, can characterize the energetic state of soil water (Pan et al., 2019; Zehe et al., 2019), they remain limited in resolving water sources, mixing pathways, and evaporation-fractionation histories (Penna et al., 2018). Recently, stable hydrogen and oxygen isotopic signatures (δ^2H and δ^{18}O) have well developed to take well advantages of their fractionation records during phase changes as water moves and exchanges with other spheres (e.g., evaporation or freezing) (Sprenger et al., 2016). For instance, by comparing the isotopic signatures in the bulk water extracted from bare surface soil and biocrust covered soil, Cao et al. (2025) observed significantly enriched δ^2H and δ^{18}O signatures in biocrust covered soil and in turn quantitatively proved the intensified soil water fractionation induced by biocrust. Given the distinct energies required across different pore domains to bind water to soil particle surfaces (Oerter et al., 2014), both the rate of atmospheric vapor exchange and the intensity of kinetic fractionation can vary markedly among pore-size classes (Gaj and McDonnell, 2019). This merits the δ^2H and δ^{18}O composition as a credible protocol to quantitatively trace the water cycling pathways across different soil pore domains (Mueller et al., 2014; Sprenger et al., 2018), and in turn their roles at soil profile and slope scales. By mixing isotopically "light" and "heavy" water in sequence into a homogenized sandy loam soil to simulate drying and rewetting, Bowers et al. (2020) pioneered in recording the prolonged mixing time in the pool of water extracted at high tension over daily timescale. Dusek and Vogel (2024) also claimed that the isotopic composition of pore water is governed by a complex pore-size effect, but they merely based on indirect inferences from bulk-soil isotope patterns together with theoretical considerations of adsorption- and pore-size-dependent isotope fractionation. Beyond δ^2H and δ^{18}O, deuterium excess (d-excess) has also been widely used to diagnose non-equilibrium kinetic fractionation and hydrological mixing processes (Dansgaard, 1964), such as evaporation imprints and water mixing histories along soil profiles (Hamani et al., 2024). Although d-excess can provide complementary information to indicate the relative differences in evaporative fractionation and hydrological history, it remains quite challenging and thus scarcely succeeded in separately obtaining and determining the δ^2H and δ^{18}O signatures of soil water stored in different pore domains/depths/positions as in the field conditions.

The black soil region in the northeastern part of China is characterized by rolling topography (Liu et al., 2023b). Thanks to the cold climate conditions (Liu et al., 2021) and high soil organic matter content (Wang et al., 2022), local soil had developed a well-connected structure with complex pore hierarchy (Peng et al., 2024). Yet, as the breadbasket of China, repeated tillage practices and seasonal erosion events had systematically reshaped soil pore structure and thus soil water recharge pathways and retention behaviors through soil profile and across slope positions (Li et al., 2021; Zhu et al., 2023; Yuan and Fan, 2024). Therefore, to resolve the complex soil water cycling at different scales in sloped field, bulk soil was sampled from different depths at different slope positions from a typical rolling slope. By subjecting individual bulk samples to high-speed centrifugation, we managed to step-wisely collect the soil water stored in five differently sized pores, enabling to actually measure and quantitatively compare the variations of pore-water δ^2H and δ^{18}O. We aimed to: (1) quantitatively identify the isotopic differentiation of pore water across five size classes and discuss the pore-specific variations in evaporative fractionation and retention time; (2) determine how soil depth and slope position reshape the spatial distribution of soil pore water, and in turn resolve the hierarchical water partitioning processes across different scales in sloped field.

2. Materials and methods

2.1. Study area

The study area is located in the Hebei watershed at Heshan Farm, Nenjiang, Heilongjiang Province, China (125°15′45.71″–125°20′46.79″ E, 48°59′03.71″–49°02′35.70″ N), a representative agricultural watershed in the rolling black soil region of Northeast China (Wang et al., 2024; Fig. 1a). The Hebei watershed covers approximately 28.0 km^2 and comprises nine small sub-catchments (Wang et al., 2023). Elevation ranges from 317 to 399 m a.s.l., and the landscape is characterized by long and gentle slopes, with typical gradients of 1.7%–10.5% and slope lengths of 500–4000 m (Zhang et al., 2025). Local agricultural fields are predominately covered with black soil, classified as Udic Isohumosols in the Chinese Soil Taxonomy and Udic Mollisols in the U.S. Soil Taxonomy. The mean annual precipitation is approximately 534 mm, most of which occurs between June and September. The average annual air temperature over the past 20 years was 1.8 °C (Hu et al., 2024). Seasonal freeze–thaw is pronounced in this region, during late autumn and early spring. The area has been cultivated for more than 60 years, typically

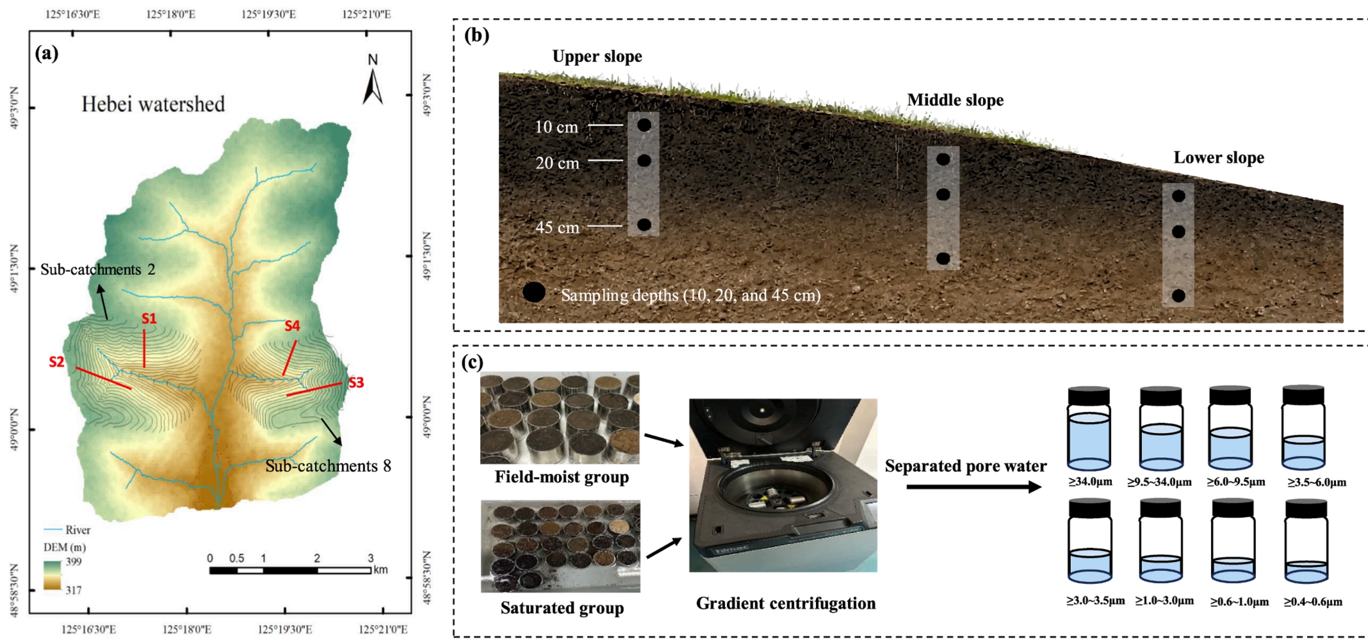

Fig. 1. Research area and experimental design: (a) location of the Hebei watershed study area; (b) sampling scheme across slope positions and soil depths; (c) experimental design for soil pore water collection.

under a maize–soybean rotation (Liu et al., 2011). To provide the meteorological context for the soil pore water observations, daily air temperature and precipitation records for the year preceding soil sampling (July 2024–June 2025) were obtained from the Nenjiang meteorological station (WMO station 50557; 49.17° N, 125.23° E; 243 m a.s.l.), the nearest national meteorological station to the study area. These records were summarized as monthly mean air temperature and monthly total precipitation and are presented in Table S1 in the Supplementary Material.

2.2. Soil sampling

Sub-catchments 2 and 8 within the Hebei watershed, respectively with an area of 3.59 and 2.30 km^2, were selected for field sampling (Fig. 1a). In each sub-catchment, two slopes oriented approximately perpendicular to each other were selected: S1 and S2 in Sub-catchment 2, and S3 and S4 in Sub-catchment 8 (Fig. 1a). Three sampling positions were selected along each slope at intervals of 200 m, hereafter termed as Upper, Middle, and Lower slope position. This sampling protocol resulted in 12 sampling points across the four slopes. At each sampling point, soil cores were seperately collected from three depths: 0–10, 10–20, and 30–45 cm (Fig. 1b).

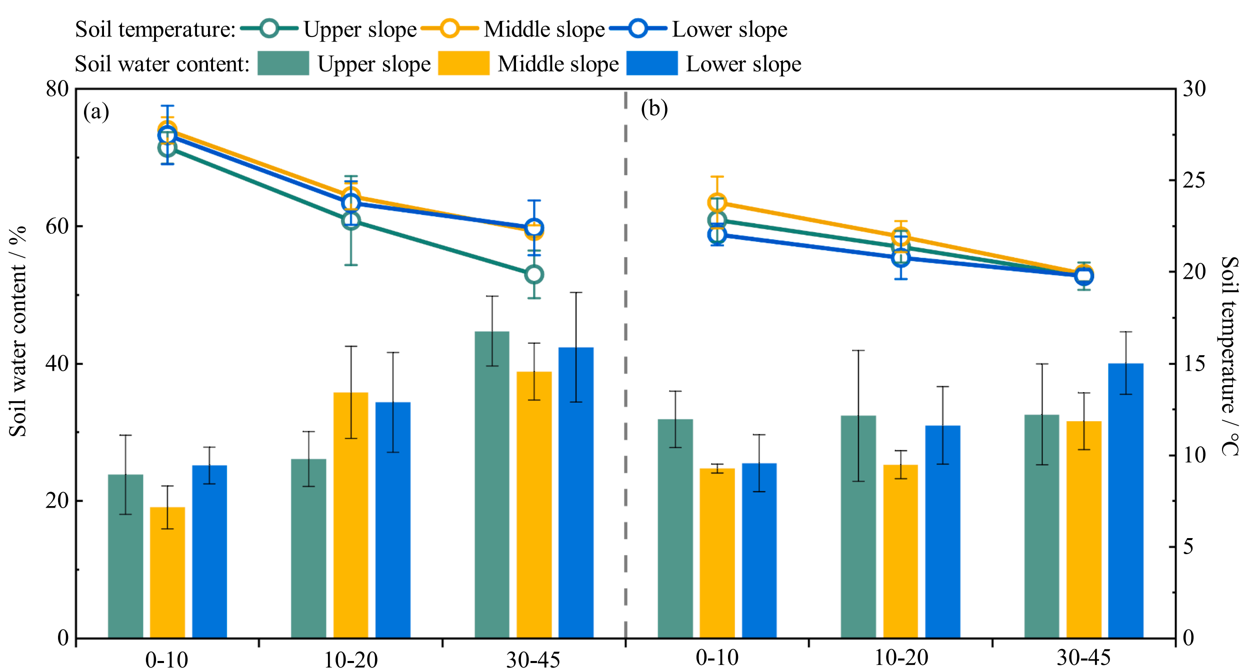

Fig. 2. Soil temperature and soil water content at the study site in the Hebei watershed: (a) Sub-catchment 2; (b) Sub-catchment 8.

Before soil sampling, soil temperature and volumetric water content were monitored *in-situ* from July 1 to July 3, 2025, respectively at three depths at each of the Upper, Middle, and Lower slope position. The monitoring records showed that soil temperature generally decreased with depth, whereas soil water content increased, and that Sub-catchment 2 generally had higher soil water content than Sub-catchment 8 (Fig. 2). Based on such field hydrothermal context, soil sampling was conducted on July 3, 2025.

At each sampling point, three undisturbed soil cores were collected from each depth using stainless-steel cutting rings (each ring of 50 mm in height, 50.46 mm in inner diameter and a volume of approximately 100 cm^3). The cultivated topsoil in the study area generally extends to a depth of 20 cm, whereas local surveys indicate that the black soil layer in the Heshan Farm watershed is approximately 44–50 cm thick (Liu et al., 2024c). Therefore, the 0–10 and 10–20 cm intervals represented the cultivated topsoil, while the 30–45 cm interval represented the deeper part of the black soil layer. Although the thickness of the black soil layer varied slightly among slope positions because of hillslope erosion and deposition, all three sampling intervals remained within the black soil layer and did not reach the parent material. The sampled soils were predominantly characterized by a silt loam texture, and their selected properties are presented in Table 1.

2.3. Experimental design

The undisturbed bulk soil cores were divided into two subgroups (Fig. 1c): (1) The soil cores from the first subgroup were rewetted with distilled water to reach saturation and then subjected to stepwise high-speed centrifugation. The mass of each soil core was recorded after centrifugated at each speed to calculate the amount of water released from the corresponding pore size range, based on which the equivalent pore diameters were calculated from the centrifugal potentials corresponding to the applied rotational speeds. For more details, please refer to Subsection 2.4. (2) The bulk soil cores from the second subgroup were maintained at their field moisture content to preserve the natural distribution of pore water at the time of sampling and were then subjected to stepwise high-speed centrifugation. The pore water discharged at each centrifugation speed was collected and then used to determine and analyze pore water δ^2H and $\delta^{18}O$ signatures. For more details on isotopic measurement and calculation, please refer to Subsection 2.5. For both subgroups, no artificial isotopic tracers were added to the soil cores.

Table 1
Selected soil properties by slope position and depth.

Slope position	Depth (cm)	Bulk density (g cm^{-3})	Sand (%)	Silt (%)	Clay (%)	SOM (g kg^{-1})
Upper slope	10	1.27 ± 0.10	16.36 ± 12.42	72.03 ± 9.24	11.61 ± 3.55	54.4
	20	1.37 ± 0.18	14.53 ± 9.66	72.79 ± 6.24	12.68 ± 4.28	49.7
	45	1.50 ± 0.06	14.29 ± 13.93	75.15 ± 11.52	10.56 ± 2.57	45.0
Middle slope	10	1.24 ± 0.23	9.89 ± 4.42	77.91 ± 2.94	12.20 ± 2.31	50.9
	20	1.32 ± 0.15	17.50 ± 14.42	70.12 ± 11.08	12.38 ± 7.45	46.5
	45	1.37 ± 0.20	16.06 ± 11.55	74.02 ± 9.56	9.92 ± 2.50	42.1
Lower slope	10	1.38 ± 0.15	35.34 ± 21.24	55.68 ± 18.69	8.97 ± 2.95	38.8
	20	1.43 ± 0.18	28.39 ± 40.36	61.52 ± 34.29	10.10 ± 6.59	36.8
	45	1.41 ± 0.33	25.28 ± 32.15	65.60 ± 26.93	9.12 ± 5.23	34.7

Note: Values are mean ± SD.

2.4. Stepwise centrifugation and pore size classification

For the first subgroup, the saturated soil cores were subjected to stepwise high-speed centrifugation to generate progressively higher matric suction, releasing water from larger pores at lower speeds and from smaller pores at higher speeds. Eight speeds of 900, 1700, 2200, 2800, 3100, 5300, 6900, and 8100 r min^{-1} were applied for 30, 45, 60, 60, 60, 90, 90, and 90 min, respectively (Yang et al., 2021; Table 2). The temperature was maintained at 19 °C throughout the centrifugation. After each centrifugation step, the saturated soil cores were weighed immediately. After the completion of the eight speeds, the soil remaining in each ring was transferred to a pre-weighed aluminum box and oven-dried at 105 °C to constant dry mass. Soil bulk density was calculated from the dry soil mass and the ring volume. The residual volumetric water content at each suction level was calculated from the dry soil mass, ring volume, and cumulative water loss.

The matric suction levels corresponding to the eight centrifugation speeds are listed in Table 2. The equivalent pore diameter at each suction level was determined using the capillary equation (Eq. (1)):

$$d_i = \frac{4\gamma cos\alpha}{\psi_i} \quad (1)$$

where d_i is the equivalent pore diameter (m), γ is the water–air interfacial surface tension (N m^{-1}), α is the water–air contact angle, and ψ_i is the positive magnitude of matric suction (Pa) at the ith centrifugation step. At the centrifugation temperature of 19 °C, γ was set to 0.07289 N m^{-1}. Assuming circular capillaries and complete wetting ($\alpha \approx 0^\circ$), Eq. (1) can be expressed in practical units as:

$$d_i\,(\mu m) \approx \frac{291.6}{\psi_i(kPa)} \quad (2)$$

The commonly used relationship $d(\mu m) \approx 300/\psi\,(kPa)$ is the rounded form of Eq. (2) and was used to define the operational pore diameter boundaries listed in Table 2.

For two consecutive suction levels corresponding to equivalent pore diameters d_1 and d_2, and residual volumetric water contents θ_1 and θ_2, respectively, where $d_1 > d_2$ and $\theta_1 > \theta_2$, the relative pore volume represented by the water released within $d_2 < d < d_1$ was calculated as (Eq. (3)):

$$P_{d_2-d_1} = \frac{\theta_1 - \theta_2}{\theta_s} \quad (3)$$

Where $P_{d_2-d_1}$ is the relative pore volume represented by the water released within this pore diameter interval, θ_1 and θ_2 are the residual volumetric water contents at two consecutive suction levels, and θ_s is the saturated volumetric water content. Water remaining after the highest centrifugation suction was assigned to the finest pore class below the final equivalent pore diameter boundary.

The pore sizes were then rounded up and classified into five pore size

Table 2
Centrifugation settings used for pore-size separation.

Rotation speed (r min^{-1})	Duration (min)	Suction (cm)	Equivalent pore diameter(μm)	Pore-size class
900	30	88.8	≥ 34.0	Macropores
1700	45	316.6	9.5–34.0	Mesopores
2200	60	530.3	6.0–9.5	Small pores
2800	60	859	3.5–6.0	Micropores
3100	60	1053	3.0–3.5	
5300	90	3018	1.0–3.0	
6900	90	5216	0.6–1.0	
8100	90	7189	0.4–0.6	Fine pores
Residue	–	–	< 0.4	

Note: Equivalent pore diameters were rounded; each interval includes its lower bound.

classes as listed in Table 2, following Cameron and Buchan (2006), Lu et al. (2014) and Zaffar and Lu (2015). We must acknowledge that the pore size classification applied in this study was more to practically compare pore water distribution and variations of isotopic compositions among different slope positions or profile layers. It did not represent a universal pore size classification protocol. After the high-speed centrifugation, the soil core deformation was $< 10\%$, indicating that the soil core volume did not remain constant during centrifugation. Such volume compression may alter void ratio and pore size distribution (Hu et al., 2013; Liu et al., 2024b), yet we merely employed this protocol to obtain pore water and compare the relative changes of pore water properties among samples from different slope positions or soil layers, rather than as an accurate description of soil water retention curves or reconstructure of pore volume distribution.

2.5. Pore water isotope measurement and d-excess calculation

Soil cores in the second subgroup were maintained at field moisture content and centrifuged using the same speeds and durations as the saturated subgroup. Water released at each step was not just weighed, but also collected and then analyzed for δ^2H and $\delta^{18}O$ using a cavity ring-down spectroscopy water isotope analyzer (Picarro L2130-i, Picarro Inc., USA). Raw isotope values were calibrated using laboratory reference waters normalized to the VSMOW-SLAP scale (Gonfiantini, 1978), and expressed in per mil (‰) (Eq. (4)). Analytical precision was better than $\pm$ 0.5‰ for δ^2H and $\pm$ 0.1‰ for $\delta^{18}O$.

$$\delta = \left(\frac{R_{sample}}{R_{standard}} - 1\right) \times 1000(‰) \tag{4}$$

where R_{sample} and $R_{standard}$ were the ratios of heavy to light isotopes in sample pore water and standard water, respectively. For hydrogen isotopes, $R = {}^2H/{}^1H$; for oxygen isotopes, $R = {}^{18}O/{}^{16}O$. The δ values of international Vienna Standard Mean Ocean Water (VSMOW) were 0‰ for both $\delta^{18}O$ and δ^2H.

Deuterium excess (d-excess) was used as a complementary isotope parameter to evaluate relative differences in evaporative fractionation and water mixing history, and was calculated as follows (Eq. (5)):

$$d - \text{excess} = \delta^2H - 8\delta^{18}O \tag{5}$$

For each extracted water sample, d-excess was calculated from the measured δ^2H and $\delta^{18}O$ and assigned to the operational pore-size class corresponding to that centrifugation step.

The Global Meteoric Water Line (GMWL; $\delta^2H = 8\delta^{18}O + 10$; Craig, 1961) and the Qiqihar Local Meteoric Water Line (LMWL; $\delta^2H = 7.59\delta^{18}O - 0.14$; Wang et al., 2020) were used as global and regional meteoric reference lines, respectively. The Qiqihar LMWL was derived from monthly precipitation isotope records from the Qiqihar station of the Global Network of Isotopes in Precipitation. These lines served as meteoric references for comparing the relative departure and cumulative evaporative imprint of pore water among pore-size classes, soil depths, and slope positions.

2.6. Data analysis

Data analysis was conducted using MATLAB (MathWorks, USA) and Excel 2021 (Microsoft, USA), and figures were prepared using Origin 2022 (OriginLab, USA). The differences in δ^2H, $\delta^{18}O$, and d-excess among slope positions, soil depths, and pore size classes were evaluated using one-way analysis of variance (ANOVA). When the ANOVA result was significant, multiple comparisons were performed using the least significant difference (LSD) test at $P < 0.05$.

3. Results

3.1. Pore size composition and pore water distribution in undisturbed soil cores

Soil pore size composition and pore water distribution varied markedly across slope positions and soil depths (Fig. 3). Overall, Micropores and Fine pores were predominant, accounting for 51.6% – 91.0% of the total pore space. Pore water was also concentrated mainly in these smaller pore (< 6 μm) domains, which together accounted for approximately 83.5% of total pore water. Along the soil profile, Macropores generally decreased with depth, whereas smaller pore classes became increasingly dominant, with pronounced variations in pore structure across the soil profile (Fig. 3). At the Upper slope position, the proportion of Fine pores increased from 45.3% at 10 cm to 53.8% at 20 cm, and then to 61.05% at 45 cm (Fig. 3a, 3d and 3 g). The Fine pores at 45 cm were 15.75% more than those at 10 cm (Fig. 3a and 3g). Consistently, the proportion of pore water stored in Fine pores increased from 77.8% to 88.9% throught depths (Fig. 3a and 3g).

Across slope positions, the proportion of larger pore classes was generally lower at the Lower slope than at the Upper slope and Middle slope (Fig. 3). At the layer of 20 cm, for example, Macropores respectively accounted for 20.4%, 12.2%, and 6.99% of the total pore space at the Upper, Middle, and Lower slope (Fig. 3d, 3e and 3f). The proportion of Macropores at the Lower slope was 13.41% lower than that at the Upper slope (Fig. 3d and 3f). In contrast, the proportion of pore water associated with those pores (size > 34 μm) increased from 37.7% at the Upper slope to 51.9% at the Middle slope, and then to 61.1% at the Lower slope (Fig. 3d, 3e and 3f). The centrifugation-derived soil pore water properties reported in this section were used only for comparisons among samples, and therefore cannot represent the actual soil water retention curves.

3.2. Distribution of pore-water δ^2H and $\delta^{18}O$ across pore size classes, soil depths and slope positions

Across the four selected slopes, δ^2H ranged from –81.96‰ to –51.42‰, with a mean of –66.65‰, whereas $\delta^{18}O$ ranged from –11.49‰ to –5.54‰, averaging at –8.55‰ (Fig. 4d). The scatter plot of δ^2H and $\delta^{18}O$ illustrates a clear linear relationship, where most samples scattered below and to the right of the Global Meteoric Water Line and the Qiqihar LMWL (Fig. 4d). Across the five pore-size classes, the δ^2H and $\delta^{18}O$ increased as pore size became finer (Fig. 4c and 4 g), both of which reached the maximum values in the finest pores (δ^2H: –64.5‰; $\delta^{18}O$: –7.9‰) and minimized in the Mesopores (δ^2H: –69.12‰; $\delta^{18}O$: –9.31‰). Across the soil profile, the δ^2H decreased by 3.52‰ and $\delta^{18}O$ by 0.88‰ from 10 to 45 cm depth (Fig. 4b and 4f). Along the three slope positions, both the δ^2H and $\delta^{18}O$ decreased significantly by approximately 7.45‰ and 1.64‰ as the elevation descended (Fig. 4a and 4e), with the decline in δ^2H being greater than that in $\delta^{18}O$.

3.3. Distribution of pore water d-excess across different pore size classes

Among all pore-size classes, the pore-water d-excess generally decreased in finer pores, but not linearly. After averaging at 3.41‰ in the Macropores (≥ 34 μm), the d-excess peaked at 5.13‰ in the Mesopores (9.5 – 34 μm), and then significantly declined to –0.704‰ in the Fine pores (< 0.6 μm) (Fig. 5). Similar patterns were observed for all the four selected slopes, but the pore-specific variations were most pronounced on S3 in Sub-catchment 8 (2.96‰ to –5.67‰, Fig. 5c), and least evident on S2 in Sub-catchment 2 (merely differenced by 4.72‰, Fig. 5b). Between the two sub-catchments, the average pore-water d-excess in Sub-catchment 2 (i.e., S1 and S2) was 1.27‰ and 4.73‰ (Fig. 5a and 5b), significantly higher than those in Sub-catchment 8 (–1.17‰ for S3 and 2.3‰ for S4) (Fig. 5c and 5d).

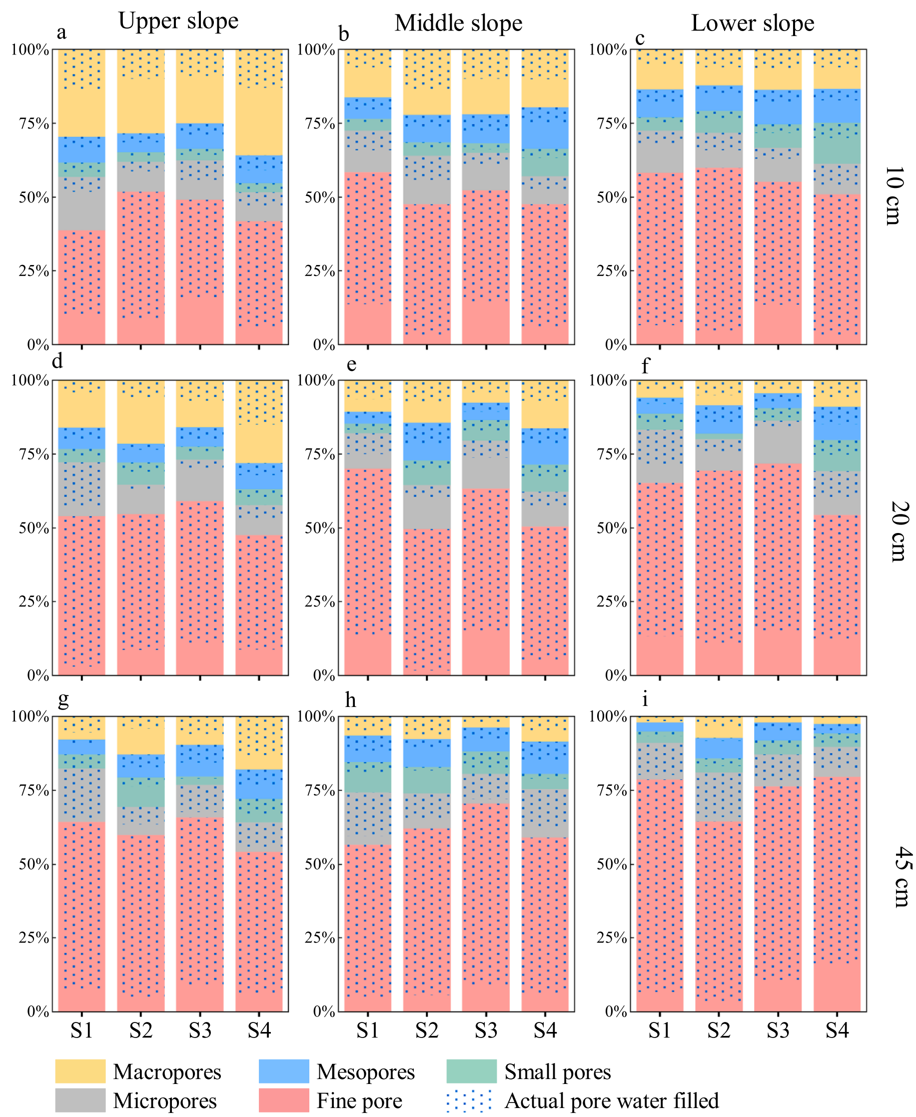

Fig. 3. Relative proportions of pore size classes and actual pore water filling across slope positions, soil depths, and the four observed slopes in the Hebei watershed. Panels (a–c), (d–f), and (g–i) represent 10, 20, and 45 cm. Columns indicate Upper, Middle, and Lower slopes, and bars denote the four observed slopes (S1–S4). Colors represent pore size classes, and hatched areas indicate the pore proportion that was actually filled with water at the sampling time.

3.4. *Distribution of pore water d-excess across soil depths*

Across soil depths, the soil pore water d-excess generally increased in deeper soil layers. After ranging from –2.58‰ to 2.88‰ at 10 cm, d-excess increased to –0.03‰ to 6.74‰ at 45 cm, suggesting progressively weaker evaporative influence with depth (Fig. 6). Similar depth-related increases were observed for the four selected slopes, but the magnitude of variation differed among slopes. The strongest depth variations were observed on S4 in Sub-catchment 8, where d-excess increased from –0.52‰ at 10 cm to 4.01‰ at 45 cm. The least depth variations appeared on S3 in Sub-catchment 8, where d-excess varied only from –2.58‰ to –0.03‰ (Fig. 6c and 6d).

Between the two sub-catchments, the average pore-water d-excess in Sub-catchment 2 was 2.998‰, significantly higher than that in Sub-catchment 8 (0.567‰). The maximum value was observed at 45 cm on S2 in Sub-catchment 2 (12.96‰), whereas the minimum value occurred at 10 cm on S3 in Sub-catchment 8 (–12.98‰) (Fig. 6b and 6c).

3.5. *Distribution of pore water d-excess over slope positions*

Along the slope positions, the soil pore water d-excess generally increased from the Upper to Lower slope, with an average difference of 5.67‰ (Fig. 7). Although similar increasing patterns were observed across the four selected slopes (Fig. 7), the variations were unequal: 5.90‰ for S1, 4.60‰ for S2, 4.76‰ for S3, and 7.42‰ for S4. More frankly, the mean d-excess was significantly higher in Sub-catchment 2 (5.67‰) than in Sub-catchment 8 (–0.84‰). The variations of d-excess among slope positions were relatively small on S2 in Sub-catchment 2 (Fig. 7b), but were much more pronounced on S4 in Sub-catchment 8 (Fig. 7d).

4. Discussion

4.1. *Pore architecture and pore water filling defined the physical basis of soil water storage*

The disproportionally more water stored in the Micropores and Fine pores (51.6%–91.0% of total space *vs.* 83.5% of total water) (Fig. 3), suggests that most water in the undisturbed soil was not stored in the coarser and more conductive pore domain, but in the smaller pores with stronger capillary and matric retention. This pattern is physically consistent with the pore-size control on soil water retention (Jarvis,

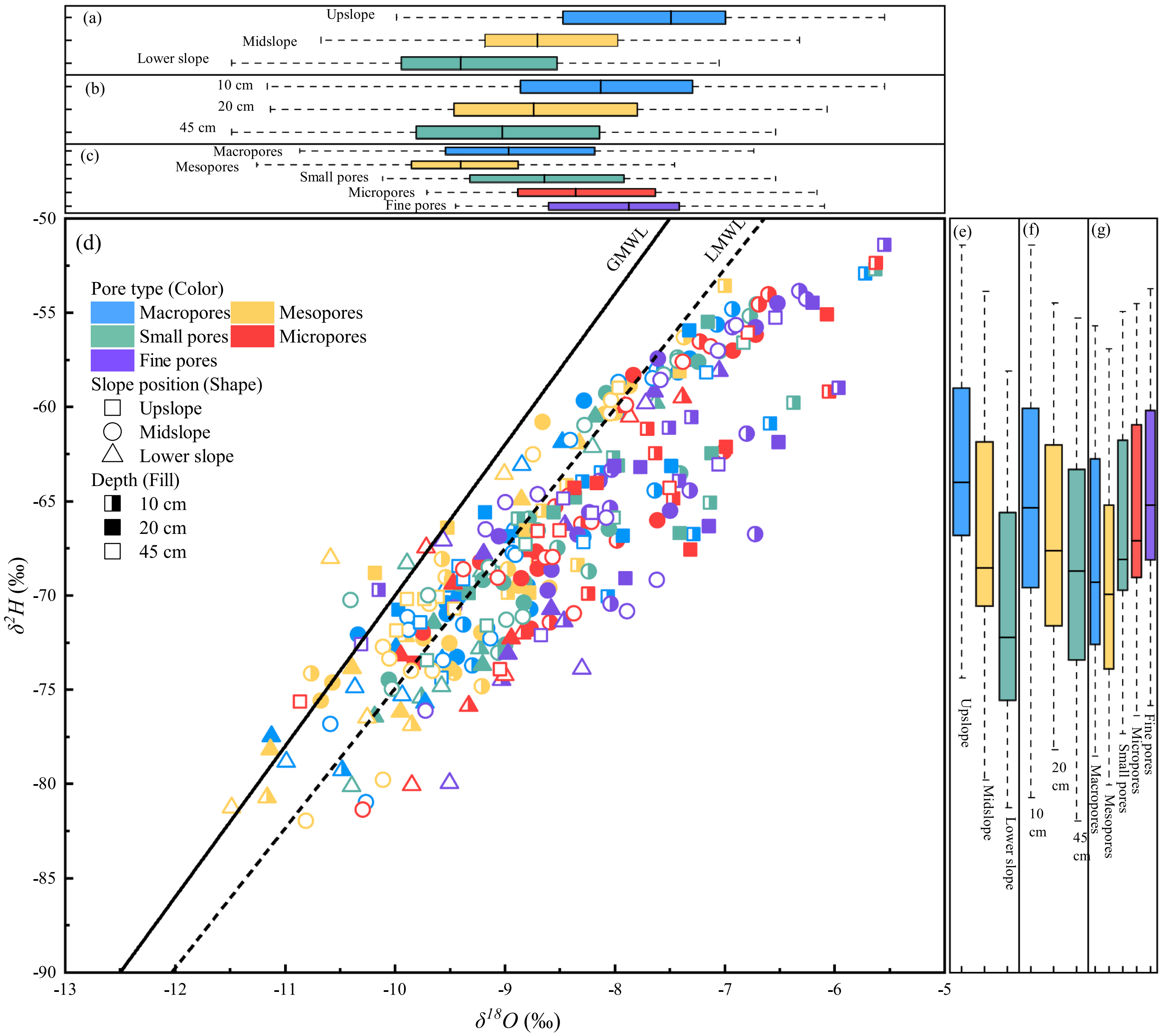

Fig. 4. Box plots of soil pore water δ^{18}O (a–c) and δ^{2}H (e–g), and the dual isotope plot (d), for samples from the Hebei watershed. Panel (d) shows the Global Meteoric Water Line (GMWL; $\delta^{2}H = 8\delta^{18}O + 10$) and the Qiqihar Local Meteoric Water Line (LMWL; $\delta^{2}H = 7.59\delta^{18}O - 0.14$), which were used as global and regional meteoric reference lines. Box plots indicate the median, interquartile range, and minimum–maximum values.

2007; Rabot et al., 2018), where Macropores appeared to be more relevant for short-term water transport and Micropores and Fine pores were the dominant water storage space. Such pore-specific variations were also evident across soil depths, where the Fine pores increased from 45.3% at 10 cm to 61.05% at 45 cm at the Upper slope position, but the water filled in those Fine pores increased from 77.8% to 88.9% (Fig. 3). While tillage disturbance, root channels, biological activities, and repeated wetting–drying in the Upper layer may help maintain relatively coarser pores, the Lower layer susceptible to compaction, aggregate rearrangement, and reduced biological pore formation was collectively favorable for finer pores and stronger water retention (Shaheb et al., 2021; Lucas et al., 2022). Nevertheless, across varying slope positions, the reduction of Macropores from 20.4% at the Upper slope to only 6.99% at the Lower slope did not result in less pore water actually filling in those Macropores, but an increase from 37.7% to 61.1% (Fig. 3). This suggests that pore function was not only determined by pore-size abundance, but also by whether a given pore domain was filled and connected under specific topographic conditions. The accumulation of water in depressed positions, deposition of finer soil particles and poor drainage may have allowed the coarser pores to remain highly frequently water filled (Dymond et al., 2021).

4.2. Pore-scale retention regulated isotopic differentiation among pore size classes

The consistently enhanced δ^{2}H and δ^{18}O signatures as the pore size became finer (Fig. 4c and 4 g) were primarily because the pore-specific physical constraints, together with the different abundance of pore domains (Fig. 3), jointly regulated the pore water mobility, residence time, and exposure to evaporative kinetic fractionation (Dusek and Vogel, 2024). For the coarse pores, e.g., Macropores > 34 μm, the fast infiltration and transport rates allowed recent precipitation to replenish water more efficiently (Radolinski et al., 2022), resulting in greater mobility, shortened residence time and in turn reduced exposure to

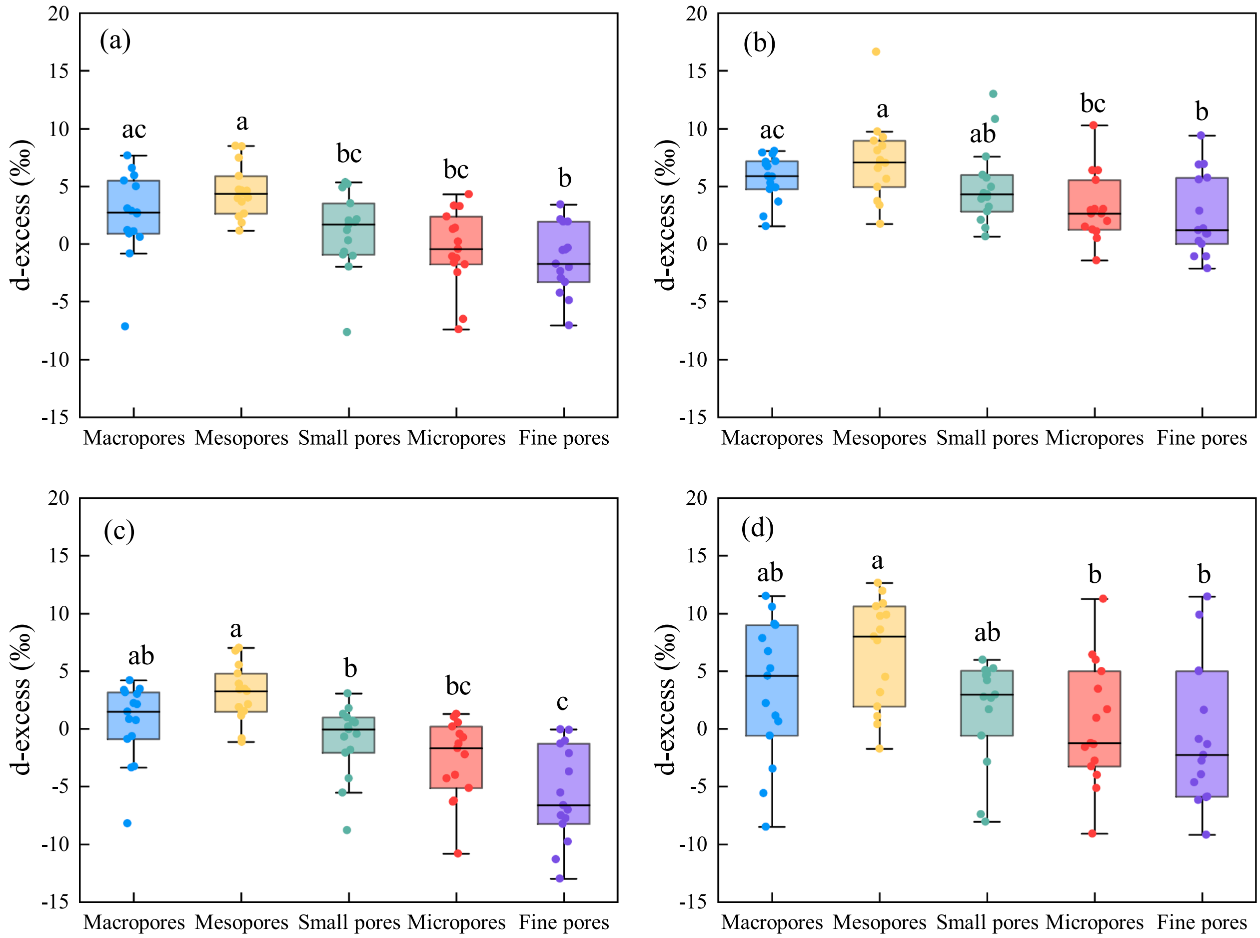

Fig. 5. Distribution of pore water d-excess among different pore types across the four study slopes. (a, b) S1 and S2 in Sub-catchment 2; (c, d) S3 and S4 in Sub-catchment 8. The box plot represents the minimum and maximum, the 25% and 75% quartiles, and the median. Different lowercase letters indicate significant differences at $P < 0.05$.

evaporative fractionation (Wang et al., 2021). Consequently, the δ^2H and δ^{18}O signatures of the water stored in Macropores plotted closer to the Qiqihar LMWL than those of water stored in finer pores (Fig. 4d). As the pore size progressively decreased, the capillary and adsorptive constraints on water became stronger, where the enhanced matric forces limited water mobility (Bowers et al., 2020), slowed down its exchange with surrounding soil water, prolonged its residence time (Sprenger et al., 2019), and consequently exposed the water in smaller pores to more advanced evaporative fractionation over longer term (old water) (Fig. 4c, 4 g and 5). Accordingly, the δ^2H and δ^{18}O signatures of the water stored in Fine pores ($<$ 0.6 μm) deviated away from the LMWL, ranging from –79.95‰ to –51.42‰ and from –10.31‰ to –5.54‰ (Fig. 4c, 4d and 4 g). Yet, when represented by the d-excess, although in general declining with finer pore sizes, it did not follow a linear pattern, but appeared to peak in the Mesopores (9.5 ~ 34 μm) for all the four slopes (Fig. 5). This suggests that the water with the greatest effective transport potential was not necessarily stored in the coarsest pores, but may have resided within a functional pore-size range (i.e., Mesopores) that could receive recharge efficiently and remain hydrologically mobile and meanwhile avoiding excessive exposure to vapor exchange. This collectively resulted in d-excess in the Mesopores being approximately 4.31‰ higher than in the Fine pores (Fig. 5).

The significantly different pore water cycling rates as quantitatively evidenced by the isotopic compartmentalization in this study generally agreed well with Dusek and Vogel (2024) and Xu et al., (2025), jointly advocating that the water stored in Fine pores was not mixed or recharged as fast as that in coarse pores during rainfall/irrigation events. Although not compared with groundwater or rainfall over different temporal resolutions as conducted in Dusek and Vogel (2024), our studies managed to systematically decipher the systematical variations of isotopic compartmentalization in pore-water in a full range of pore size classes rather than just differentiating mobile or bulk water. Yet, we must acknowledge that pore-water isotopes are not only the results from pore-structural differences in evaporative fractionation and recharge rates, but reflecting the integrated information from the differentiated responses of water across positions, depths, and pore-size classes to rainfall input, evaporative loss, and internal mixing (Ibarra and Evaristo, 2024). The day-scale differences in mixing time among pore water sequentially extracted at low-, mid- and high-tension as pioneered by Xu et al. (2025) further highlight the sensitivity of pore-water isotopic signatures to rainfall, drought or irrigation events. This warrants future studies to verify the pore water isotopic differentiation across varying size classes over a wider range of soils and water-input regimes (Canet-Martí et al., 2023; Wardak et al., 2022), as well as integrate with long-term *in-situ* monitoring to better resolve the role of pore water cycling in slope-scale hydrological partitioning.

4.3. *Slope position and soil depth reshaped pore-water isotopic fractionation*

The linearly depleted δ^2H and δ^{18}O (Fig. 4b and 4f) yet significantly enhanced d-excess (Fig. 6) as observed from 10 cm to 45 cm was primarily because the Upper soil (10 cm) was directly exposed to the atmosphere, subjected to more intensively to solar radiation, air

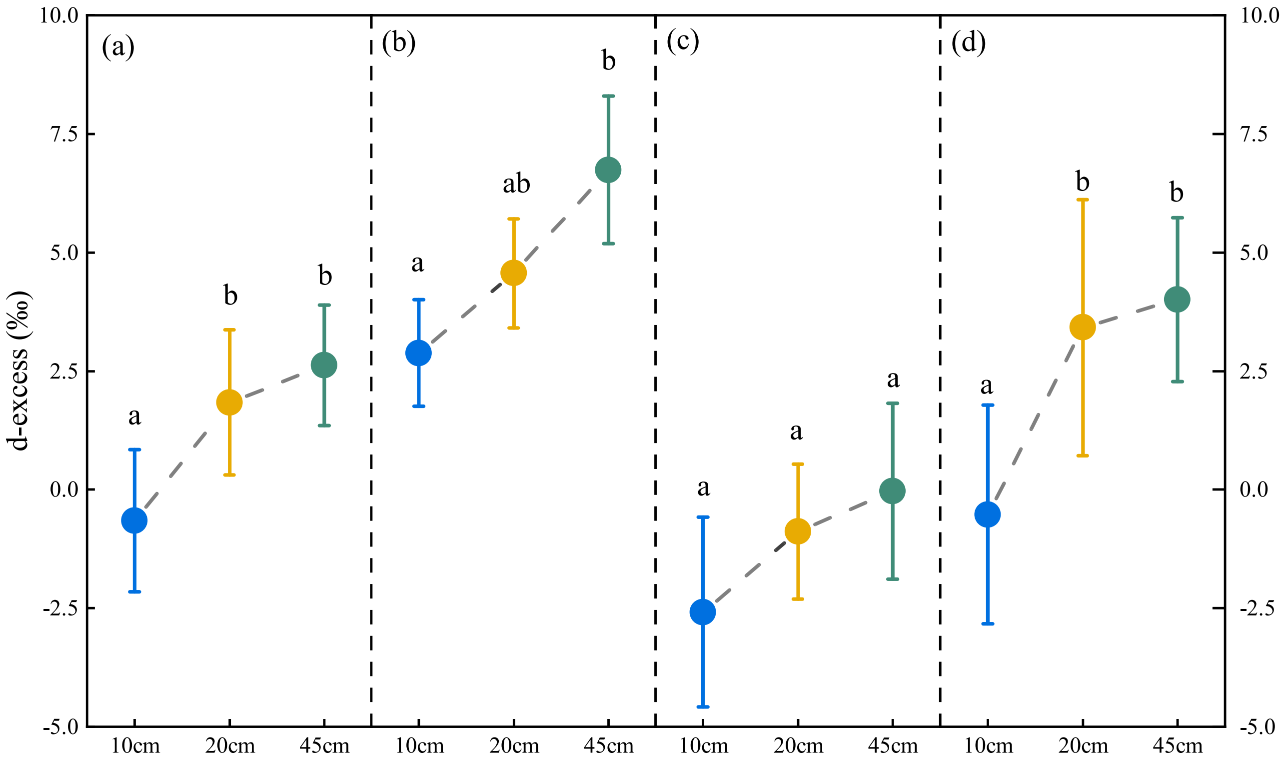

Fig. 6. Distribution of pore water d-excess among different soil depths across the four study slopes. (a, b) S1 and S2 in Sub-catchment 2; (c, d) S3 and S4 in Sub-catchment 8. Different lowercase letters indicate significant differences at $P < 0.05$.

temperature variations, and wind speed changes (Liu et al., 2024a; Lyu and Wang, 2021). This not only preferentially removed the lighter isotopes (^{1}H and ^{16}O), but also resulted in enriched ^{2}H and ^{18}O and significantly lower d-excess in the residual soil water in the Upper layer, as compared to the local meteoric water line (LMWL) (Fig. 4b, 4f and 6). Meanwhile, the soil pore structure became gradually compacted at depths (Fig. 3). On the one hand, the tightly compacted pore structure in the deeper layer may partly contribute to reduced evaporative fractionation, especially when considering that the relatively high organic matter content of the study soil may also help to preserve deep soil water for longer retention time (Yang et al., 2014). On the other hand, as water (mainly from precipitation) infiltrated downward into deeper soil, the largely suppressed evaporative fractionation in the 45 cm retained the isotopic signatures closer to those of the LMWL (Fig. 4d) and in turn preserved with higher d-excess (Fig. 6). Similar isotopic fractionation can also be observed among topographic positions. The isotopically enriched soil pore water with lower d-excess at the Upper slope (Fig. 4a, 4f, 7) was mainly resulted from the less intensified erosion, thus limited contribution area for runoff-enabled soil–water recharge (mainly from precipitation), and in turn higher susceptibility to evaporative loss. In addition, the greater proportions of Macropores and Mesopores at the upper slope (Fig. 3a) favored rapid infiltration, making pore water more readily exposed to atmospheric exchange and intensified evaporative fractionation. By contrast, at the Lower slope position, since it practically functioned as a topographic depositional zone that not only received precipitation but also accumulated runoff and fine-textured sediments generated from upper contributing area (Fig. 3). Dense texture, reinforced soil water content and thus weakened aeration jointly suppressed evaporative fractionation and consequently resulted in significantly higher pore-water d-excess at the Lower slope position (Fig. 7).

The depth-related increase in d-excess observed in this study was consistent with Yong et al. (2020) and Zhu et al. (2022), which collectively confirmed that the evaporative enrichment was strongest in surface soil water and weakened markedly with depth. The contrast d-excess between the Upper and Lower slope positions further highlights the additional influence of topographic controls (as illustrated in the conceptual scheme in Fig. 8). Our observations that Upper slope soil water was more strongly affected by evaporation and therefore exhibited more pronounced isotopic alteration are in good line with Zhang et al. (2023), who reported that downslope with young and event water depended strongly on subsurface structure and lateral flow pathways. This interpretation is also validated by the greater soil water but lower temperature at deeper layer and at Lower slope position observed from the *in-situ* records (Fig. 2). Similar variations in soil moisture across soil depths and slope positions have also been reported by Jarecke et al. (2021) and Dymond et al. (2021). Unlike the conventional studies where the hillslope and profile-scale water cycling was primarily inferred from soil-moisture profiles or Richards-equation-based simulations (Bauser et al., 2022), this study quantitatively distinguished and visualized the extent of evaporative fractionation in soil pore water across topographic and profile positions. Given the likelihood of intensified precipitation unpredictability and hillslope hydrological heterogeneity under future climate conditions and land-use conversion modes (Li et al., 2009), such quantitative discrimination of pore-water cycling rates is urgently needed to develop holistic understanding of water partitioning patterns across different terrain features and varying land use types.

4.4. Implications and limitations

Although the pore-size classes separated in this study could not fully represent the soil pore networks under field conditions, the evidently unequal isotopic signatures among different pore domains clearly demonstrate that soil water should not be interpreted as a single reservoir. Crude changes in bulk soil water could not distinguish the coexistence of rapidly renewed water in Macropores (Renée Brooks et al., 2010), actively exchangeable water in Mesopores, or strongly retained water in Fine pores. The hierarchical partitioning of soil water across different scales in the sloped field demonstrated that soil depth and slope

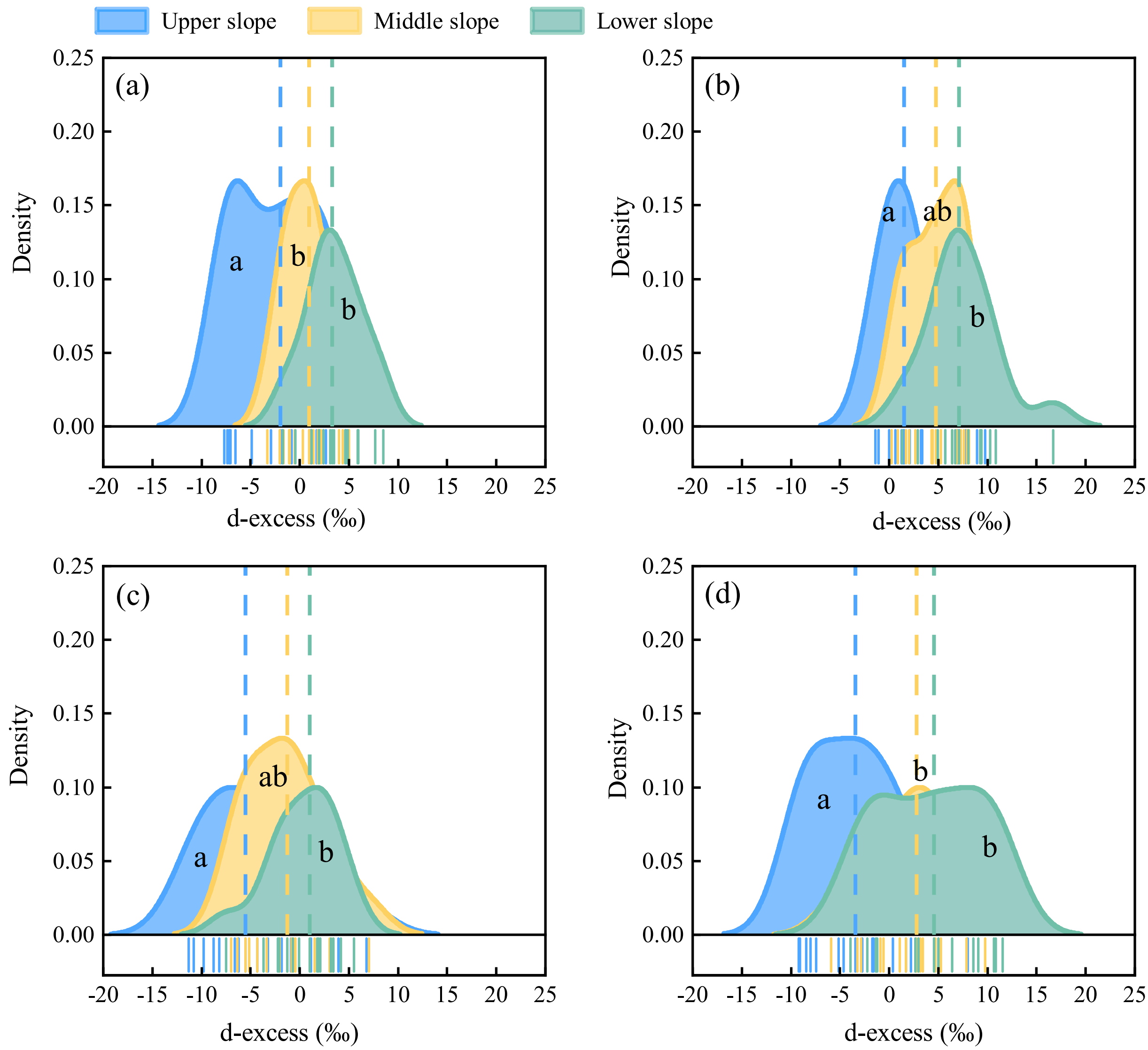

Fig. 7. Distribution of pore water d-excess among different slope positions across the four study slopes. (a, b) S1 and S2 in Sub-catchment 2; (c, d) S3 and S4 in Sub-catchment 8. The dashed lines indicate median values; solid lines represent the values for each sample ($n = 45$ independent samples). Different lowercase letters indicate significant differences at $P < 0.05$.

position shaped the local hydrothermal and structural setting, whereas pore structure and pore water filling provided the immediate physical basis for water retention, mobility, and isotopic differentiation within that setting. As conceptually illustrated in Fig. 8, this study helps to advance our current understanding by providing pore-scale quantitative evidence and emphasizing that ecohydrological fractionation may begin within the soil matrix itself, rather than only among broad compartments such as soil water, plant water (Sprenger et al., 2018), groundwater (Adams et al., 2020) or stream water (Dusek and Vogel, 2024). The redistribution and thus restructure of soil pores along hillslopes and across profiles further regulate the water cycling rates among layers and slope positions, although outperformed by the topographically and downwardly depressed evaporative fractionation at profile and slope scale (Fig. 8). Moreover, we also acknowledge that the centrifuge-based pore-water separation used here was more advantageous in isolating pore-specific isotope signals, but it failed to reproduce the non-equilibrium exchange, preferential flow activation, and temporal connectivity among pores during repeated drying-rewetting cycles over rainfall or irrigation events. In addition, this study was based on cross-sectional sampling at a single time point, and thus could not determine how the observed pore-domain fractionation evolves over seasons or years. Under future climate conditions, changing rainfall intensity, longer dry intervals, and stronger event-scale recharge (Pendergrass et al., 2017; Feldman et al., 2024) may further interfere the relative contributions of Macropore flow rates, Mesopore exchange rates, and Fine pore retention ability. Therefore, long-term *in-situ* profile monitoring, together with pore-fractionated isotopic signature and pore-network imaging would help further disentangle how pore-scale water storage and exchange regulate hillslope-scale evaporation and plant water availability.

5. Conclusion

To examine how pore class, soil depth and slope position jointly shaped soil water partitioning and isotope fractionation, soil water stored in differently sized pores were separately extracted, and compared their δ^2H, $\delta^{18}O$ and d-excess across depths and slope positions. Micropores and Fine pores predominantly accounted for 51.6%–91.0% of the total pore space and stored about 83.5% of the extracted water. The enrichment of δ^2H and $\delta^{18}O$ toward finer pores, together with the highest d-excess in Mesopores, showed that pore water did not cycle at the same rates. Under the sampled conditions, Mesopores

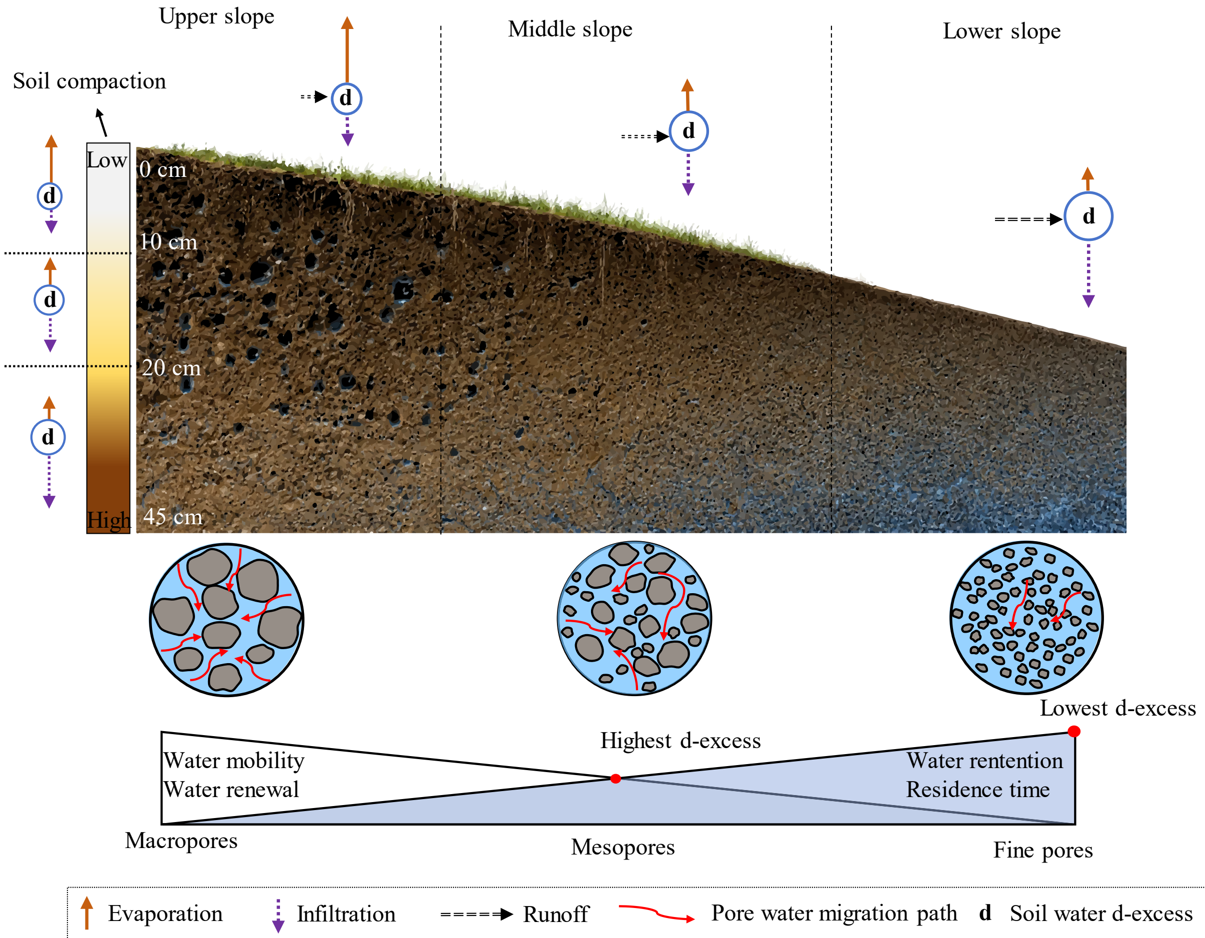

Fig. 8. The diagram illustrates the potential influence of different slopes, soil depths and pore structures on the distribution characteristics of soil pore water and hydrogen and oxygen isotope concentrations.

appeared to serve as actively mobile water domain susceptible to less evaporation, whereas Fine pores stored more tightly retained water with advanced evaporative fractionation. The higher d-excess at deeper layer and Lower slope position further revealed the determined role of localized evaporative fractionation in slope-scale water partitioning, as relative to the efficient recharge of downward infiltration and abundant accumulation of upper land runoff. Although based on cross-sectional sampling and predetermined pore size classes, the hierarchical water partitioning evidenced by varying soil water pore isotopic signatures in this study advocates more advanced distinguish in pore water cycling rates, instead of crude soil water enrichment or depletion, to better understand hillslope hydrological processes and their responses to erosion events or tillage practices under changing climate conditions.

CRediT authorship contribution statement

Jinzhuo Li: Writing – review & editing, Writing – original draft, Investigation, Formal analysis, Data curation. **Xianwen Li:** Writing – review & editing. **Mo Li:** Writing – review & editing. **Liu Liu:** Writing – review & editing. **Xiaorong Wei:** Writing – review & editing. **Yaxian Hu:** Writing – review & editing, Project administration, Funding acquisition, Conceptualization.

Declaration of competing interest

The authors declare that they have no known competing financial interests or personal relationships that could have appeared to influence the work reported in this paper.

Acknowledgement

This study was financially supported by the National Key Research and Development Program of China (2024YFD1502000) and the National Natural Science Foundation of China (42477373, 52279049).

Appendix A. Supplementary data

Supplementary data to this article can be found online at https://doi.org/10.1016/j.jhydrol.2026.136200.

Data availability

Data will be made available on request.

References

Adams, R.E., Hyodo, A., SantaMaria, T., Wright, C.L., Boutton, T.W., West, J.B., 2020. Bound and mobile soil water isotope ratios are affected by soil texture and mineralogy, whereas extraction method influences their measurement. Hydrol. Process. 34, 991–1003. https://doi.org/10.1002/hyp.13633.

Bauser, H.H., Kim, M., Ng, W., Bugaj, A., Troch, P.A., 2022. Richards equation at the hillslope scale: can we resolve the heterogeneity of soil hydraulic material properties? Water Resour. Res. 58, e2022WR032294. https://doi.org/10.1029/2022WR032294.

Beven, K., Germann, P., 2013. Macropores and water flow in soils revisited: review. Water Resour. Res. 49, 3071–3092. https://doi.org/10.1002/wrcr.20156.

Bonetti, S., Wei, Z., Or, D., 2021. A framework for quantifying hydrologic effects of soil structure across scales. Commun. Earth Environ. 2, 107. https://doi.org/10.1038/s43247-021-00180-0.

Bowers, W.H., Mercer, J.J., Pleasants, M.S., Williams, D.G., 2020. A combination of soil water extraction methods quantifies the isotopic mixing of waters held at separate tensions in soil. Hydrol. Earth Syst. Sci. 24, 4045–4060. https://doi.org/10.5194/hess-24-4045-2020.

Cameron, K.C., Buchan, G.D., 2006. Porosity and pore size distribution. Encyclopedia of Soil Science 2, 1350–1353.

Canet-Martí, A., Morales-Santos, A., Nolz, R., Langergraber, G., Stumpp, C., 2023. Quantification of water fluxes and soil water balance in agricultural fields under different tillage and irrigation systems using water stable isotopes. Soil Tillage Res. 231, 105732. https://doi.org/10.1016/j.still.2023.105732.

Cao, Y., Xiao, B., Sun, F., Heitman, J., 2025. Enriched stable hydrogen and oxygen isotopes in biocrusts unveil their critical roles in mediating ecohydrological processes of drylands. Plant and Soil 514, 1903–1921. https://doi.org/10.1007/s11104-025-07497-1.

Chandrasekhar, P., Kreiselmeier, J., Schwen, A., Weninger, T., Julich, S., Feger, K.-H., Schwärzel, K., 2018. Why we should include soil structural dynamics of agricultural soils in hydrological models. Water 10, 1862. https://doi.org/10.3390/w10121862.

Chen, C., Zou, X., Singh, A.K., Zhu, X., Zhang, W., Yang, B., Jiang, X., Liu, W., 2021. Effects of hillslope position on soil water infiltration and preferential flow in tropical forest in southwest China. J. Environ. Manage. 299, 113672. https://doi.org/10.1016/j.jenvman.2021.113672.

Craig, H., 1961. Isotopic variations in meteoric waters. Science 133, 1702–1703. https://doi.org/10.1126/science.133.3465.1702.

Dansgaard, W., 1964. Stable isotopes in precipitation. Tellus 16, 436–468. https://doi.org/10.1111/j.2153-3490.1964.tb00181.x.

De Lima, R.P., Rolim, M.M., Toledo, M.P.S., Tormena, C.A., Da Silva, A.R., Silva, E., I.A. C., Pedrosa, E.M.R.,, 2022. Texture and degree of compactness effect on the pore size distribution in weathered tropical soils. Soil Tillage Res. 215, 105215. https://doi.org/10.1016/j.still.2021.105215.

Dusek, J., Vogel, T., 2024. Isotopic signatures and soil water partitioning in a humid temperate forest catchment: implications for the 'two-water-worlds' hypothesis. J. Hydrol. 632, 130893. https://doi.org/10.1016/j.jhydrol.2024.130893.

Dymond, S.F., Wagenbrenner, J.W., Keppeler, E.T., Bladon, K.D., 2021. Dynamic hillslope soil moisture in a mediterranean montane watershed. Water Resour. Res. 57, e2020WR029170. https://doi.org/10.1029/2020WR029170.

Fatichi, S., Or, D., Walko, R., Vereecken, H., Young, M.H., Ghezzehei, T.A., Hengl, T., Kollet, S., Agam, N., Avissar, R., 2020. Soil structure is an important omission in earth system models. Nat. Commun. 11, 522. https://doi.org/10.1038/s41467-020-14411-z.

Feldman, A.F., Feng, X., Felton, A.J., Konings, A.G., Knapp, A.K., Biederman, J.A., Poulter, B., 2024. Plant responses to changing rainfall frequency and intensity. Nature Reviews Earth & Environment 5, 276–294. https://doi.org/10.1038/s43017-024-00534-0.

Floriancic, M.G., Allen, S.T., Kirchner, J.W., 2024. Young and new water fractions in soil and hillslope waters. Hydrol. Earth Syst. Sci. 28, 4295–4308. https://doi.org/10.5194/hess-28-4295-2024.

Gaiser, T., Perkons, U., Küpper, P.M., Puschmann, D.U., Peth, S., Kautz, T., Pfeifer, J., Ewert, F., Horn, R., Köpke, U., 2012. Evidence of improved water uptake from subsoil by spring wheat following lucerne in a temperate humid climate. Field Crop Res 126, 56–62. https://doi.org/10.1016/j.fcr.2011.09.019.

Gaj, M., McDonnell, J.J., 2019. Possible soil tension controls on the isotopic equilibrium fractionation factor for evaporation from soil. Hydrol. Process. 33, 1629–1634. https://doi.org/10.1002/hyp.13418.

Gonfiantini, R., 1978. Standards for stable isotope measurements in natural compounds. Nature 271, 534–536. https://doi.org/10.1038/271534a0.

Hamani, A.K.M., Liu, J., Si, Z., Kpalari, D.F., Wang, G., Gao, Y., Ju, X., 2024. The relationship of δD and δ18O in soil water and its implications for soil evaporation across distinct rainfall years in winter wheat field in the North China Plain. Agric Water Manag 304, 109092. https://doi.org/10.1016/j.agwat.2024.109092.

He, D., Oliver, Y., Rab, A., Fisher, P., Armstrong, R., Kitching, M., Wang, E., 2022. Plant available water capacity (PAWC) of soils predicted from crop yields better reflects within-field soil physicochemical variations. Geoderma 422, 115958. https://doi.org/10.1016/j.geoderma.2022.115958.

Henrique Novotny, E., Ribeiro deAzevedo, E., De Godoy, G., Martelozo Consalter, D., Cooper, M.,, 2023. Determination of soil pore size distribution and water retention curve by internal magnetic field modulation at low field 1H NMR. Geoderma 431, 116363. https://doi.org/10.1016/j.geoderma.2023.116363.

Hu, R., Chen, Y.-F., Liu, H.-H., Zhou, C.-B., 2013. A water retention curve and unsaturated hydraulic conductivity model for deformable soils: consideration of the change in pore-size distribution. Géotechnique 63, 1389–1405. https://doi.org/10.1680/geot.12.P.182.

Hu, Y., Yuan, X., Wang, X., Song, Y., Peng, Z., Yan, B., Li, X., 2024. Unequal impacts of unidirectional freeze-thaw on different soil layers and aggregate sizes: evidenced by microbial communities and CO2 emissions. Catena 241, 108057. https://doi.org/10.1016/j.catena.2024.108057.

Ibarra, D.E., Evaristo, J., 2024. Soil pore water evaporation and temperature influences on clay mineral paleothermometry. Commun. Earth Environ. 5, 21. https://doi.org/10.1038/s43247-024-01201-4.

Jarecke, K.M., Bladon, K.D., Wondzell, S.M., 2021. The influence of local and nonlocal factors on soil water content in a steep forested catchment. Water Resour. Res. 57, e2020WR028343. https://doi.org/10.1029/2020WR028343.

Jarvis, N.J., 2007. A review of non-equilibrium water flow and solute transport in soil macropores: principles, controlling factors and consequences for water quality. European J Soil Science 58, 523–546. https://doi.org/10.1111/j.1365-2389.2007.00915.x.

Knighton, J., Souter-Kline, V., Volkmann, T., Troch, P.A., Kim, M., Harman, C.J., Morris, C., Buchanan, B., Walter, M.T., 2019. Seasonal and topographic variations in ecohydrological separation within a small, temperate, snow-influenced catchment. Water Resour. Res. 55, 6417–6435. https://doi.org/10.1029/2019WR025174.

Li, H., Zhu, H., Wei, X., Liu, B., Shao, M., 2021. Soil erosion leads to degradation of hydraulic properties in the agricultural region of Northeast China. Agr Ecosyst Environ 314, 107388. https://doi.org/10.1016/j.agee.2021.107388.

Li, Z., Liu, W., Zhang, X., Zheng, F., 2009. Impacts of land use change and climate variability on hydrology in an agricultural catchment on the Loess Plateau of China. J. Hydrol. 377, 35–42. https://doi.org/10.1016/j.jhydrol.2009.08.007.

Liu, B., Ma, R., Fan, H., 2021. Evaluation of the impact of freeze-thaw cycles on pore structure characteristics of black soil using X-ray computed tomography. Soil Tillage Res. 206, 104810. https://doi.org/10.1016/j.still.2020.104810.

Liu, F., Li, X., Shi, F., Yang, Y., Liu, M., Cao, G., 2024a. Stable isotopes reveal soil evaporation and its controlling factors in the Heihe River source area on the northeastern Qinghai-Tibetan Plateau. J. Hydrol.: Reg. Stud. 54, 101901. https://doi.org/10.1016/j.ejrh.2024.101901.

Liu, J., Leung, A.K., Dong, H., Lai, N.T., 2024b. A state-dependent bimodal soil water retention model considering evolutions of pore-scale soil–water interaction. Comput. Geotech. 175, 106704. https://doi.org/10.1016/j.compgeo.2024.106704.

Liu, J., Si, Z., Li, S., Hamani, K.M., A., Zhang, Y., Wu, L., Gao, Y., Duan, A.,, 2023a. Variations in water sources used by winter wheat across distinct rainfall years in the North China Plain. J. Hydrol. 618, 129186. https://doi.org/10.1016/j.jhydrol.2023.129186.

Liu, X., Guo, M., Zhang, X., Zhang, S., Zhou, P., Chen, Z., Qi, J., Shen, Q., 2023b. Morphological characteristics and volume estimation model of permanent gullies and topographic threshold of gullying in the rolling hilly Mollisols region of northeast China. Catena 231, 107323. https://doi.org/10.1016/j.catena.2023.107323.

Liu, X., Zhang, S., Zhang, X., Ding, G., Cruse, R.M., 2011. Soil erosion control practices in Northeast China: a mini-review. Soil Tillage Res. 117, 44–48. https://doi.org/10.1016/j.still.2011.08.005.

Lu, S.-G., Malik, Z., Chen, D.-P., Wu, C.-F., 2014. Porosity and pore size distribution of Ultisols and correlations to soil iron oxides. Catena 123, 79–87. https://doi.org/10.1016/j.catena.2014.07.010.

Lucas, M., Nguyen, L.T.T., Guber, A., Kravchenko, A.N., 2022. Cover crop influence on pore size distribution and biopore dynamics: enumerating root and soil faunal effects. Front. Plant Sci. 13, 928569. https://doi.org/10.3389/fpls.2022.928569.

Lyu, S., Wang, J., 2021. Soil water stable isotopes reveal surface soil evaporation loss dynamics in a subtropical forest plantation. Forests 12, 1648. https://doi.org/10.3390/f12121648.

McDonnell, J.J., 2014. The two water worlds hypothesis: ecohydrological separation of water between streams and trees? WIREs Water 1, 323–329. https://doi.org/10.1002/wat2.1027.

Mueller, M.H., Alaoui, A., Kuells, C., Leistert, H., Meusburger, K., Stumpp, C., Weiler, M., Alewell, C., 2014. Tracking water pathways in steep hillslopes by δ18O depth profiles of soil water. J. Hydrol. 519, 340–352. https://doi.org/10.1016/j.jhydrol.2014.07.031.

Munns, R., Day, D.A., Fricke, W., Watt, M., Arsova, B., Barkla, B.J., Bose, J., Byrt, C.S., Chen, Z., Foster, K.J., Gilliham, M., Henderson, S.W., Jenkins, C.L.D., Kronzucker, H. J., Miklavcic, S.J., Plett, D., Roy, S.J., Shabala, S., Shelden, M.C., Soole, K.L., Taylor, N.L., Tester, M., Wege, S., Wegner, L.H., Tyerman, S.D., 2020. Energy costs of salt tolerance in crop plants. New Phytol. 225, 1072–1090. https://doi.org/10.1111/nph.15864.

Nasta, P., Franz, T.E., Gibson, J.P., Romano, N., 2023. Revisiting the definition of field capacity as a functional parameter in a layered agronomic soil profile beneath irrigated maize. Agric Water Manag 284, 108368. https://doi.org/10.1016/j.agwat.2023.108368.

Oerter, E., Finstad, K., Schaefer, J., Goldsmith, G.R., Dawson, T., Amundson, R., 2014. Oxygen isotope fractionation effects in soil water via interaction with cations (Mg, Ca, K, Na) adsorbed to phyllosilicate clay minerals. J. Hydrol. 515, 1–9. https://doi.org/10.1016/j.jhydrol.2014.04.029.

Pan, T., Hou, S., Liu, Y., Tan, Q., 2019. Comparison of three models fitting the soil water retention curves in a degraded alpine meadow region. Sci. Rep. 9, 18407. https://doi.org/10.1038/s41598-019-54449-8.

Pendergrass, A.G., Knutti, R., Lehner, F., Deser, C., Sanderson, B.M., 2017. Precipitation variability increases in a warmer climate. Sci. Rep. 7, 17966. https://doi.org/10.1038/s41598-017-17966-y.

Peng, J., Wu, Y., Geng, T., Zhang, C., Wang, J., Cai, C., 2024. Soil pore dynamics and infiltration characteristics as affected by cultivation duration for Mollisol in northeast China. Geoderma 449, 117021. https://doi.org/10.1016/j.geoderma.2024.117021.

Penna, D., Hopp, L., Scandellari, F., Allen, S.T., Benettin, P., Beyer, M., Geris, J., Klaus, J., Marshall, J.D., Schwendenmann, L., Volkmann, T.H.M., von Freyberg, J., Amin, A., Ceperley, N., Engel, M., Frentress, J., Giambastiani, Y., McDonnell, J.J., Zuecco, G., Llorens, P., Siegwolf, R.T.W., Dawson, T.E., Kirchner, J.W., 2018. Ideas and perspectives: tracing terrestrial ecosystem water fluxes using hydrogen and oxygen stable isotopes – challenges and opportunities from an interdisciplinary perspective. Biogeosciences 15, 6399–6415. https://doi.org/10.5194/bg-15-6399-2018.

Rabot, E., Wiesmeier, M., Schlüter, S., Vogel, H.-J., 2018. Soil structure as an indicator of soil functions: a review. Geoderma 314, 122–137. https://doi.org/10.1016/j.geoderma.2017.11.009.

Radolinski, J., Le, H., Hilaire, S.S., Xia, K., Scott, D., Stewart, R.D., 2022. A spectrum of preferential flow alters solute mobility in soils. Sci. Rep. 12, 4261. https://doi.org/10.1038/s41598-022-08241-w.

Radolinski, J., Pangle, L., Klaus, J., Stewart, R.D., 2021. Testing the 'two water worlds' hypothesis under variable preferential flow conditions. Hydrol. Process. 35, e14252. https://doi.org/10.1002/hyp.14252.

Reddy, I.N.B.L., Kim, B.-K., Yoon, I.-S., Kim, K.-H., Kwon, T.-R., 2017. Salt tolerance in rice: focus on mechanisms and approaches. Rice Sci. 24, 123–144. https://doi.org/10.1016/j.rsci.2016.09.004.

Renée Brooks, J., Barnard, H.R., Coulombe, R., McDonnell, J.J., 2010. Ecohydrologic separation of water between trees and streams in a Mediterranean climate. Nat. Geosci. 3, 100–104. https://doi.org/10.1038/ngeo722.

Romano, N., 2014. Soil moisture at local scale: measurements and simulations. J. Hydrol. 516, 6–20. https://doi.org/10.1016/j.jhydrol.2014.01.026.

Schlüter, S., Sammartino, S., Koestel, J., 2020. Exploring the relationship between soil structure and soil functions via pore-scale imaging. Geoderma 370, 114370. https://doi.org/10.1016/j.geoderma.2020.114370.

Shaheb, M.R., Venkatesh, R., Shearer, S.A., 2021. A review on the effect of soil compaction and its management for sustainable crop production. J. Biosyst. Eng. 46, 417–439. https://doi.org/10.1007/s42853-021-00117-7.

Sprenger, M., Leistert, H., Gimbel, K., Weiler, M., 2016. Illuminating hydrological processes at the soil-vegetation-atmosphere interface with water stable isotopes. Rev. Geophys. 54, 674–704. https://doi.org/10.1002/2015RG000515.

Sprenger, M., Stumpp, C., Weiler, M., Aeschbach, W., Allen, S.T., Benettin, P., Dubbert, M., Hartmann, A., Hrachowitz, M., Kirchner, J.W., McDonnell, J.J., Orlowski, N., Penna, D., Pfahl, S., Rinderer, M., Rodriguez, N., Schmidt, M., Werner, C., 2019. The demographics of water: a review of water ages in the critical zone. Rev. Geophys. 57, 800–834. https://doi.org/10.1029/2018RG000633.

Sprenger, M., Tetzlaff, D., Buttle, J., Laudon, H., Leistert, H., Mitchell, C.P.J., Snelgrove, J., Weiler, M., Soulsby, C., 2018. Measuring and modeling stable isotopes of mobile and bulk soil water. Vadose Zone J. 17, 1–18. https://doi.org/10.2136/vzj2017.08.0149.

Sprenger, M., Tetzlaff, D., Soulsby, C., 2017. Soil water stable isotopes reveal evaporation dynamics at the soil–plant–atmosphere interface of the critical zone. Hydrol. Earth Syst. Sci. 21, 3839–3858. https://doi.org/10.5194/hess-21-3839-2017.

Vereecken, H., Amelung, W., Bauke, S.L., Bogena, H., Brüggemann, N., Montzka, C., Vanderborght, J., Bechtold, M., Blöschl, G., Carminati, A., Javaux, M., Konings, A.G., Kusche, J., Neuweiler, I., Or, D., Steele-Dunne, S., Verhoef, A., Young, M., Zhang, Y., 2022. Soil hydrology in the Earth system. Nature Reviews Earth & Environment 3, 573–587. https://doi.org/10.1038/s43017-022-00324-6.

Wang, C., Zhang, G., Zhu, P., Chen, S., Wan, Y., 2023. Spatial variation of soil functions affected by land use type and slope position in agricultural small watershed. Catena 225, 107029. https://doi.org/10.1016/j.catena.2023.107029.

Wang, G., Zhang, K., Jia, C., Zhang, Z., 2024. Physical property responses of soils subjected to different degrees of erosion and seasonal freeze-thaw cycles in Northeast China. Soil Tillage Res. 244, 106264. https://doi.org/10.1016/j.still.2024.106264.

Wang, H., Jin, J., Cui, B., Si, B., Ma, X., Wen, M., 2021. Technical note: evaporating water is different from bulk soil water in δ^2H and δ^{18}O and has implications for evaporation calculation. Hydrol. Earth Syst. Sci. 25, 5399–5413. https://doi.org/10.5194/hess-25-5399-2021.

Wang, S., Wang, Z., Heinonsalo, J., Zhang, Y., Liu, G., 2022. Soil organic carbon stocks and dynamics in a mollisol region: a 1980s–2010s study. Sci. Total Environ. 807, 150910. https://doi.org/10.1016/j.scitotenv.2021.150910.

Wang, T., Li, T.-Y., Zhang, J., Wu, Y., Chen, C.-J., Huang, R., Li, J.-Y., Xiao, S.-Y., Artemevna Blyakharchuk, T., 2020. A climatological interpretation of precipitation δ18O across Siberia and Central Asia. Water 12, 2132. https://doi.org/10.3390/w12082132.

Wardak, D.L.R., Padia, F.N., De Heer, M.I., Sturrock, C.J., Mooney, S.J., 2022. Zero tillage has important consequences for soil pore architecture and hydraulic transport: a review. Geoderma 422, 115927. https://doi.org/10.1016/j.geoderma.2022.115927.

Xu, X., Zhao, Z., Skrzypek, G., 2025. Stable isotope disequilibrium between soil bound water and soil bulk water – implications for estimations of plant water sources. J. Hydrol. 650, 132544. https://doi.org/10.1016/j.jhydrol.2024.132544.

Yang, F., Zhang, G.-L., Yang, J.-L., Li, D.-C., Zhao, Y.-G., Liu, F., Yang, R.-M., Yang, F., 2014. Organic matter controls of soil water retention in an alpine grassland and its significance for hydrological processes. J. Hydrol. 519, 3086–3093. https://doi.org/10.1016/j.jhydrol.2014.10.054.

Yang, Y., Chen, Y., Chen, J., Zhang, Z., Li, Y., Du, Y., 2021. The applicability of HYDRUS-1D to infiltration of water-repellent soil at different depths. Eur. J. Soil Sci. 72, 2020–2032. https://doi.org/10.1111/ejss.13100.

Yong, L., Zhu, G., Wan, Q., Xu, Y., Zhang, Z., Sun, Z., Ma, H., Sang, L., Liu, Y., Guo, H., Zhang, Y., 2020. The soil water evaporation process from mountains based on the stable isotope composition in a headwater basin and northwest China. Water 12, 2711. https://doi.org/10.3390/w12102711.

Yuan, C., Fan, H., 2024. Response mechanism of black soil structure to compound erosion forces in sloping farmland. Northeast China. Soil and Tillage Research 240, 106103. https://doi.org/10.1016/j.still.2024.106103.

Zaffar, M., Lu, S.-G., 2015. Pore size distribution of clayey soils and its correlation with soil organic matter. Pedosphere 25, 240–249. https://doi.org/10.1016/S1002-0160(15)60009-1.

Zehe, E., Loritz, R., Jackisch, C., Westhoff, M., Kleidon, A., Blume, T., Hassler, S.K., Savenije, H.H., 2019. Energy states of soil water – a thermodynamic perspective on soil water dynamics and storage-controlled streamflow generation in different landscapes. Hydrol. Earth Syst. Sci. 23, 971–987. https://doi.org/10.5194/hess-23-971-2019.

Zhang, J., Chen, H., Fu, Z., Wang, F., Wang, K., 2023. Towards hydrological connectivity in the karst hillslope critical zone: insight from using water isotope signals. J. Hydrol. 617, 128926. https://doi.org/10.1016/j.jhydrol.2022.128926.

Zhang, Y., Zhang, G., Zhang, N., Xing, S., Zhang, Y.i., 2025. Response of soil erosion resistance to incorporated straw affected by different microbial inoculants in the black soil region of Northeast China. Agr Ecosyst Environ 392, 109765. https://doi.org/10.1016/j.agee.2025.109765.

Zhao, X., Li, F., Ai, Z., Li, J., Gu, C., 2018. Stable isotope evidences for identifying crop water uptake in a typical winter wheat–summer maize rotation field in the North China Plain. Sci. Total Environ. 618, 121–131. https://doi.org/10.1016/j.scitotenv.2017.10.315.

Zhu, G., Yong, L., Zhao, X., Liu, Y., Zhang, Z., Xu, Y., Sun, Z., Sang, L., Wang, L., 2022. Evaporation, infiltration and storage of soil water in different vegetation zones in the Qilian Mountains: a stable isotope perspective. Hydrol. Earth Syst. Sci. 26, 3771–3784. https://doi.org/10.5194/hess-26-3771-2022.

Zhu, P., Zhang, G., Yang, Y., Wang, C., Chen, S., Wan, Y., 2023. Infiltration properties affected by slope position on cropped hillslopes. Geoderma 432, 116379. https://doi.org/10.1016/j.geoderma.2023.116379.

Liu, R., Wang, Z., Tan, Y., 2024c. The thickness of black soil layer and its influencing factors in a small watershed of typical black soil region in Northeast China (in Chinese). J. Soil Water Conserv. 38, 346–353. https://doi.org/10.13870/j.cnki.stbcxb.2024.04.024.